ELSEVIER

Journal of Chromatography A, 732 (1996) 119–132

JOURNAL OF CHROMATOGRAPHY A

Dynamic modeling of electrophoretically mediated microanalysis

Dale H. Patterson, Bryan J. Harmon, Fred E. Regnier*

Department of Chemistry, Purdue University,, West Lafayett, IN 47907-1393, USA

Received 5 September 1995; revised 2 November 1995; accepted 3 November 1995

Abstract

A dynamic model is presented for simulation of reaction-based chemical analysis of enzymes and substrates in capillary electrophoretic systems by the methodology of electrophoretically mediated microanalysis (EMMA). The mathematical model utilizes mass balance expressions describing the time-dependent effects of electromigration, chemical reaction, and diffusional band broadening upon the concentration profiles of the various reagent and product species. The model is implemented in an iterative computer program in which the capillary is segmented into arrays of bins storing the concentration profiles of each of the chemical species. During each time increment, the effects of electrophoresis, reaction kinetics, and diffusion are calculated, and the concentrations stored in the arrays are updated. The flexibility of the model to accommodate various initial capillary conditions, sample introduction methods, and voltage programming allows diverse EMMA analyses to be simulated. The simulated results are shown to be in good qualitative agreement with experimental data for zonal injection and moving boundary EMMA determinations of leucine aminopeptidase as well as an EMMA analysis of ethanol.

Keywords: Electrophoretically mediated microanalysis; Mathematical modelling; Electromigration; Band broadening; Computer simulation; Diffusion; Reaction kinetics; Ethanol; Leucine aminopeptidase; Aminopeptidases; Enzymes

1. Introduction

The methodology of electrophoretically mediated microanalysis (EMMA) allows homogeneous reaction-based chemical analysis to be performed in capillary electrophoretic systems [1–17]. In a typical EMMA experiment, differential electrophoretic mobility is utilized to merge distinct zones of analyte and analytical reagent(s) under the influence of an electric field. The analytical reaction is then allowed to proceed within the region of reagent overlap either in the presence or absence of applied potential, and the resultant product is transported to the detector under the influence of an electric field. EMMA-type methods have been reported for the enzymatic determination of both enzymes [2–10] and substrates [9–12] as well as the complexatory determination of inorganic ions [13–16].

We have previously presented mathematical models for EMMA determinations of enzymes [8–10] and substrates [9,10] using zonal [9,10] and moving boundary [8] sample introduction methods. These models have accounted for the effects of electromigration of the reagent and product species as well as reaction kinetics upon the observed product profiles. Although we have shown that there is qualitative agreement between experimental product profiles and those predicted by our static models, a dynamic model which could simulate the state of the experiment (i.e., provide concentration profiles of

*Corresponding author.

0021-9673/96/$15.00 © 1996 Elsevier Science B.V. All rights reserved
SSDI 0021-9673(95)01247-8

each reagent and product species) at any time during its course would be of greater value in the understanding and design of an EMMA analysis. The numerous EMMA methodologies which have been reported also require greater flexibility in experimental design than can be adequately described by a single static model. These parameters include the choice of initial capillary conditions (e.g., the ability to fill the capillary or buffer reservoirs with various reagents), sample introduction methods (e.g., hydrodynamic and electrokinetic zonal injections as well as electrokinetic moving boundary sample introduction), and voltage programming (e.g., time periods in the presence or absence of an applied potential). Furthermore, the static models have neglected certain factors which could significantly affect an EMMA determination, including diffusional band broadening of reagent and product zones and variability in reaction rate due to depletion of analytical reagents.

This paper reports a dynamic model of EMMA which is capable of simulating the state of the experiment at any time during its course as well as the final electropherogram. The mathematical model accounts for the time-dependent effects of electrophoresis, reaction kinetics, and diffusion upon the concentration profiles of the reagent and product species and is flexible in its ability to simulate the various experimental modes of EMMA. Validation of this dynamic model will be shown by a qualitative comparison of experimental and simulated results for the EMMA determination of enzymes and substrates utilizing both zonal and moving boundary sample introduction.

2. Mathematical model of EMMA

Since electromigration, chemical reaction, and diffusional band broadening are primary determinants of the concentration profiles of the reagents and resultant product in an EMMA determination [9], they are the principal components of our mathematical model. For each reagent and product species i at position x along the length of the capillary (i.e., $0 \leq x \leq L$ where L is the length of the capillary), a one-dimensional total mass balance equation (T) can be written as the sum of terms representing the time-dependent contributions of electromigration (E), chemical reaction (R), and diffusion (D)

$$\left[\frac{\delta C_i(x,t)}{\delta t}\right]_T = \left[\frac{\delta C_i(x,t)}{\delta t}\right]_E + \left[\frac{\delta C_i(x,t)}{\delta t}\right]_R + \left[\frac{\delta C_i(x,t)}{\delta t}\right]_D \quad (1)$$

where $C_i(x,t)$ is the concentration of i at x and time t. As described by Dose and Guiochon [17], the contents of the buffer reservoirs at each end of the capillary may be represented by defining the values of $C_i(0,t)$ and $C_i(L,t)$ for all i and t.

Electromigration can be modeled as

$$\left[\frac{\delta C_i(x,t)}{\delta t}\right]_E = -\frac{\delta F_i(x,t)}{\delta x} \quad (2)$$

where $F_i(x,t)$ is the electromigrational flux of i at x and t, which, in the presence of an electric field $E(x,t)$, is given by

$$F_i(x,t) = (\mu_{ep,i} + \mu_{eo})\, E(x,t)\, C_i(x,t) \quad (3)$$

where $\mu_{ep,i}$ is the electrophoretic mobility of i, and μ_{eo} is the electroosmotic mobility. Our simple model for electromigration further assumes that the presence of reagent or product solutes does not significantly affect the local solution conductance, and, thus, the electric field strength is constant throughout the capillary [i.e., $E(t)$]. Therefore, the electromigrational contribution to the time-dependent concentration profile of i is given by

$$\left[\frac{\delta C_i(x,t)}{\delta t}\right]_E = -(\mu_{ep,i} + \mu_{eo})\, E(t)\, \frac{\delta C_i(x,t)}{\delta x} \quad (4)$$

Since EMMA methods previously reported by our laboratory have utilized reagent and product concentrations which were low relative to the carrier electrolyte, significant effects of nonlinear behavior due to dissimilar local conductivities [18–20] have not been observed and, thus, are not considered in this model. However, the model could be extended to include this phenomenon in a manner similar to that utilized by Dose and Guiochon [17].

To illustrate the effects of reaction kinetics, the simplest enzymatic system which can be modeled is a single-substrate enzymatic reaction displaying Michaelis–Menten kinetics

$$\left[\frac{\delta[\mathrm{P}](x,t)}{\delta t}\right]_R = -\left[\frac{\delta[\mathrm{S}](x,t)}{\delta t}\right]_R = \frac{k_{\mathrm{cat}}[\mathrm{E}](x,t)[\mathrm{S}](x,t)}{K_{\mathrm{M,S}} + [\mathrm{S}](x,t)} \quad (5)$$

where $[\mathrm{P}](x,t)$, $[\mathrm{S}](x,t)$, and $[\mathrm{E}](x,t)$ are the concentrations of product, substrate, and enzyme, respectively, at x and t, and k_{cat} and $K_{\mathrm{M,S}}$ are the turnover number and Michaelis constant, respectively, for the enzyme and substrate. Since enzyme is not consumed by the reaction, it does not exhibit a reaction-dependent term; i.e.,

$$\left[\frac{\delta[\mathrm{E}](x,t)}{\delta t}\right]_R = 0 \quad (6)$$

More complex kinetic systems (e.g., enzymes requiring multiple substrates) can be easily accommodated by altering the form of Eq. 5.

Diffusion can be modeled by a one-dimensional form of Fick's Law

$$\left[\frac{\delta C_{i,x}}{\delta t}\right]_D = D_i \frac{\delta^2 C_i(x,t)}{\delta x^2} \quad (7)$$

where D_i is the diffusion coefficient of i. Although this model does not explicitly include other band broadening mechanisms observed in capillary electrophoretic methods (e.g., thermal effects or solute interactions with the capillary wall), their effects can be incorporated into the diffusion coefficient utilized in the model. However, in EMMA, band broadening can also occur due to the mechanism of complex formation. If the electrophoretic mobility of the enzyme–substrate complex differs from that of either uncomplexed species, the observed mobility of that species is dependent upon the concentration of the corresponding ligand [21,22]. Furthermore, as modeled by Avila et al. [22] for affinity capillary electrophoresis, the peak broadens in the region of intermediate migration velocity if the rate of equilibration between species of different mobilities is relatively slow. Due to the inavailability of necessary kinetic constants (i.e., formation and dissociation rates for enzyme–substrate and enzyme–product complexes), this mechanism is not considered in the current model. However, the use of experimentally determined apparent diffusion coefficients ($D_{\mathrm{app},i}$) and electrophoretic mobilities ($\mu_{\mathrm{ep,app},i}$) based upon experimental peak variances [23] and migration times, respectively, allows the net effects of this phenomenon to be approximated.

Thus, a model describing the time-dependent effects of electromigration, chemical reaction, and diffusion upon the concentration profiles of enzyme, substrate, and product for an enzymatic system displaying Michaelis–Menten kinetics can be obtained by substitution of the appropriate terms into Eq. 1

$$\left[\frac{\delta[\mathrm{E}](x,t)}{\delta t}\right]_T = -(\mu_{\mathrm{ep,app,E}} + \mu_{\mathrm{eo}})E(t)\frac{\delta[\mathrm{E}](x,t)}{\delta x} + D_{\mathrm{app,E}}\frac{\delta^2[\mathrm{E}](x,t)}{\delta x^2} \quad (8)$$

$$\left[\frac{\delta[\mathrm{S}](x,t)}{\delta t}\right]_T = -(\mu_{\mathrm{ep,app,S}} + \mu_{\mathrm{eo}})E(t)\frac{\delta[\mathrm{S}](x,t)}{\delta x} - \frac{k_{\mathrm{cat}}[\mathrm{E}](x,t)[\mathrm{S}](x,t)}{K_{\mathrm{M,S}} + [\mathrm{S}](x,t)} + D_{\mathrm{app,S}}\frac{\delta^2[\mathrm{S}](x,t)}{\delta x^2} \quad (9)$$

$$\left[\frac{\delta[\mathrm{P}](x,t)}{\delta t}\right]_T = -(\mu_{\mathrm{ep,app,P}} + \mu_{\mathrm{eo}})E(t)\frac{\delta[\mathrm{P}](x,t)}{\delta x} + \frac{k_{\mathrm{cat}}[\mathrm{E}](x,t)[\mathrm{S}](x,t)}{K_{\mathrm{M,S}} + [\mathrm{S}](x,t)} + D_{\mathrm{app,P}}\frac{\delta^2[\mathrm{P}](x,t)}{\delta x^2} \quad (10)$$

Based upon the choice of initial capillary conditions [i.e., $C_i(x,0)$ for all i and x], buffer reservoir contents [i.e., $C_i(0,t)$ and $C_i(L,t)$ for all i and t], and voltage programming [i.e., $E(t)$], this model offers great flexibility to simulate numerous EMMA experiments. Furthermore, the electropherogram may be obtained by monitoring $C_i(x_{\mathrm{det}},t)$ (where x_{det} is the detection position) for each detectable species.

3. Experimental

3.1. Computer implementation of mathematical model

Since no exact solution of these differential equations was possible, the solution was obtained in an iterative fashion utilizing incremental values of x and t defined by the spatial (Δx_{res}) and temporal (Δt_{res}) resolution, respectively, of the simulation. Based upon the user-defined spatial resolution, the capillary was segmented into an array of N_{bins} adjacent bins of uniform width

$$N_{bins} = \frac{L}{\Delta x_{res}} \tag{11}$$

A concentration profile array, in which each array element (i.e., $C_i[j]$ where $0 \leq j \leq N_{bins}$) contained the concentration of i at the corresponding spatial position within the capillary, was then generated for each reagent and product species. The reservoirs at the ends of the capillary were represented by cells of constant content defined by the user, and detection was achieved by monitoring the single bin in each species' concentration profile array corresponding to the detection position of the capillary. During each time increment, the program cycled through specific subroutines which calculated the individual effects of the three principal components of the mathematical model (i.e. electromigration, chemical reaction, and diffusional band broadening) and updated the concentration profile arrays for each reagent and product species. The number of cycles (N_{cycles}) required to simulate a period of time (t_{sim}) was determined by the user-defined temporal resolution

$$N_{cycles} = \frac{t_{sim}}{\Delta t_{res}} \tag{12}$$

In the electromigration subroutine, the concentration profile array elements for each species were simply shifted a number of bins (Δj_i) corresponding to their distance of electromigration during the time increment as determined by the species' apparent electrophoretic mobility as well as the electroosmotic mobility, strength and polarity of the applied electric field, and temporal and spatial resolution

$$\Delta j_i = \frac{(\mu_{ep,app,i} + \mu_{eo})\, E\, \Delta t_{res}}{\Delta x_{res}} \tag{13}$$

For each capillary position containing non-zero concentrations of each of the species required for chemical reaction, the reaction kinetics subroutine calculated reaction-induced changes in concentration during the time increment. For the Michaelis–Menten system, an integrated rate expression for substrate concentration was solved iteratively

$$[S]_f[j] = k_{cat}[E][j]\, \Delta t_{res} + [S]_i[j] - K_M \ln\frac{[S]_f[j]}{[S]_i[j]} \tag{14}$$

where $[S]_i[j]$ and $[S]_f[j]$ were, respectively, the initial and final substrate concentrations, and $[E][j]$ was the enzyme concentration of array element j during the time increment. The updated product concentration at that capillary position was then determined by the calculated change in substrate concentration

$$[P]_f[j] = [P]_i[j] + ([S]_i[j] - [S]_f[j]) \tag{15}$$

where $[P]_i[j]$ and $[P]_f[j]$ were, respectively, the initial and final product concentrations of array element j during the time increment. For kinetic systems where an integrated expression was not possible, the initial rate law was utilized to estimate concentration changes.

The diffusional band broadening subroutine allowed each array element containing a non-zero concentration of a reagent or product to diffuse independently during each time increment. The diffusion of a single bin was accomplished by applying that species' gaussian "diffusional profile," which was an array of probabilities representing the fraction of an individual array element's concentration which would diffuse into adjacent bins during the time increment. The diffusional profile accounted for diffusion into adjacent bins spanning $\pm 4\sigma$ [i.e., $-4(2\, D_{app,i}\, \Delta t_{res})^{1/2} \leq \Delta j \leq 4(2\, D_{app,i}\, \Delta t_{res})^{1/2}$] from the array element to which it was applied. The fraction of the array element's concentration which would diffuse into each particular adjacent bin ($P_i[\Delta j]$) was calculated from the species' apparent diffusion coefficient and the temporal and spatial resolution

$$P_i[\Delta j] = \frac{e^{-\frac{(\Delta j\, \Delta x_{res})^2}{4 D_{app,i}\, \Delta t_{res}}}}{2(\pi D_{app,i}\, \Delta t_{res})^{1/2}} \tag{16}$$

The results of the independent diffusion of each array element were superimposed to yield the net effect of diffusional band broadening upon each species' concentration profile during the time increment.

Upon initiating the simulation, the user defined the physical and chemical system by entering simulation parameters (e.g., spatial and temporal resolution), experimental parameters (e.g., capillary dimensions and electroosmotic mobility), and information about each reagent and product species (e.g., initial concentration or activity, apparent electrophoretic mobility, apparent diffusion coefficient, absorptivity, and kinetic constants). From this point, the simulation was written in a manner attempting to mimic the options available to the user in a physical EMMA experiment. Thus, the user initially specified the solutions to be placed in the capillary and the anodic and cathodic buffer reservoirs, and, after the program calculated diffusional profiles and initialized concentration profile arrays for each reagent and product species, a menu offered the following options to the user: (1) allow system to sit in absence of electric field for specified time period; (2) apply specified potential for specified time period; (3) change specified buffer reservoir composition; (4) perform hydrodynamic injection for specified height or pressure and specified time at specified end of capillary; and (5) terminate experiment. The user could also view the current concentration profiles of each reagent or product species or the current electropherogram at any time during the simulated experiment.

Various combinations of these menu options allowed for flexibility in the simulation of numerous experimental procedures. For example, although there existed no specific subroutine for performing a zonal electrokinetic injection, one could be accomplished simply by changing the composition of the appropriate buffer reservoir to the desired solution, selecting the option to apply a potential for the desired time of injection, and then returning the buffer reservoir to its initial composition. During the application of the electric field, the program cycled through the subroutines representing electromigration, reaction kinetics, and diffusion. However, since the mathematical model described does not address hydrodynamic displacement, an additional subroutine was created to simulate hydrodynamic injections.

The simulation was written in C, compiled using the Borland (Monterrey, CA, USA) Turbo C environment, and executed on Pentium-based 90 MHz PCs. Quinn–Curtis (Needham, MA, USA) Huge Virtual Arrays and Numerical Methods Toolbox for Borland/Turbo C (version 2.0) was utilized to overcome the DOS limitation of 640 kB base memory for data storage, and screen and printer graphics were written with the assistance of Quinn–Curtis Science and Engineering Tools for Borland/Turbo C (version 8.0). Specific simulation parameters are detailed in Table 1. All parameters were determined experimentally with the exception of Michaelis constants which were taken from [24] and [25] for the determinations of leucine aminopeptidase (LAP; EC 3.4.1.1) and ethanol, respectively. At the spatial and temporal resolutions stated in Table 1, the program ran in approximately real time.

3.2. Experimental EMMA determinations

The EMMA determinations of LAP and ethanol depicted in Fig. 2, Fig. 4 and Fig. 6, respectively, were performed as previously described in [8] and [10], respectively.

4. Results and discussion

Although the flexibility of the mathematical model to accommodate various initial capillary conditions, sample introduction methods, and voltage programming allows numerous modes of EMMA to be simulated, the following discussion is limited to the simulation of three representative EMMA determinations previously reported by our laboratory. Whereas only selected concentration profiles are presented to illustrate the methods, the program displays concentration profiles over the entire capillary for each reagent and product species following each time increment thus providing a "snapshot by snapshot" view of the complete evolution of the simulated experiment. In the concentration profiles presented, in order that all reagent and product concentrations can be represented relative to a single y-axis, the concentrations of each reagent species are scaled relative to their initial concentrations while product concentrations are depicted relative to the maximum value observed for the concentration

Table 1
Simulation and experimental parameters for EMMA determinations depicted in Figs. 1–6

Parameter	Figures	
	1–4	5–6
Simulation parameters		
Δx_{res} (cm)	0.005	0.0025
Δt_{res} (s)	1.0	2.0
Experimental parameters		
L (cm)	24	24
l (cm)	19.4	19.4
μ_{eo} ($cm^2 V^{-1} s^{-1}$)	$5.0 \cdot 10^{-4}$	$3.8 \cdot 10^{-4}$
Enzyme parameters		
Identity	LAP	ADH
k_{cat} [E] ($U ml^{-1}$)	0.2	60
$\mu_{ep,app}$ ($cm^2 V^{-1} s^{-1}$)	$-1.0 \cdot 10^{-4}$	$-1.1 \cdot 10^{-4}$
D_{app} ($cm^2 s^{-1}$)	$5 \cdot 10^{-6}$	$8 \cdot 10^{-6}$
ϵb(AU M^{-1})	0	0
Substrate parameters		
Identity	L-Leucine-*p*-nitroanalide	Ethanol
[S] (M)	0.004	0.01
$\mu_{ep,app}$ ($cm^2 V^{-1} s^{-1}$)	$1.0 \cdot 10^{-4}$	0
D_{app} ($cm^2 s^{-1}$)	$6 \cdot 10^{-5}$	$4 \cdot 10^{-5}$
ϵb(AU M^{-1})	0	0
$K_{M,S}$ (mM)	1.1	12
Cofactor parameters		
Identity	N/A	NAD^+
[C] (M)	N/A	0.01
$\mu_{ep,app}$ ($cm^2 V^{-1} s^{-1}$)	N/A	$-0.9 \cdot 10^{-4}$
D_{app} ($cm^2 s^{-1}$)	N/A	$3 \cdot 10^{-5}$
ϵb(AU M^{-1})	N/A	0
$K_{M,C}$ (mM)	N/A	0.15
$K_{M,SC}$ (mM^2)	N/A	10
Detectable product parameters		
Identity	*p*-Nitroanaline	NADH
$\mu_{ep,app}$ ($cm^2 V^{-1} s^{-1}$)	0	$-1.8 \cdot 10^{-4}$
D_{app} ($cm^2 s^{-1}$)	$8 \cdot 10^{-5}$	$3 \cdot 10^{-5}$
ϵb(AU M^{-1})	16	10

l=Separation length of capillary (distance from anodic inlet to detection position). ϵb=Molar absorptivity·path length constant. N/A=not applicable.

profiles shown in each figure (i.e., $3.7 \cdot 10^{-5}$, $4.5 \cdot 10^{-4}$, and $1.3 \cdot 10^{-3}$ M in Fig. 1, Fig. 3, and Fig. 5, respectively).

4.1. Simulation of zonal injection EMMA determination of LAP

The most prevalent application of the EMMA methodology has been the kinetic determination of enzymes utilizing zonal sample introduction [2–10]. Fig. 1 and Fig. 2 depict the simulation of the EMMA determination of LAP previously reported [8] utilizing this technique. LAP was assayed by its hydrolysis of L-leucine-*p*-nitroanilide to form L-leucine and *p*-nitroaniline, which was detected by its unique absorbance at 405 nm.

Since LAP possessed a lower net migration velocity than L-leucine-*p*-nitroanilide, the substrate was

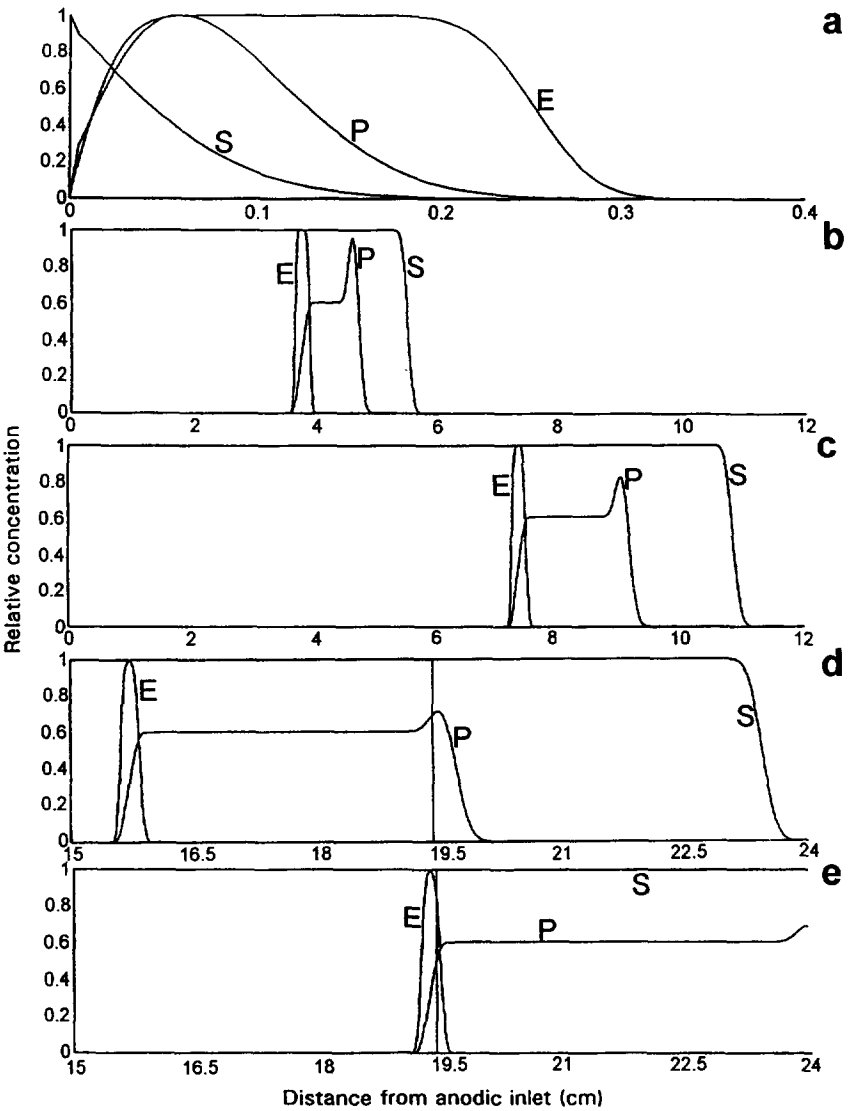

Fig. 1. Simulation of the zonal injection EMMA determination of LAP (a) immediately prior to the application of potential and following the application of 300 V cm^{-1} for (b) 30, (c) 60, (d) 130, and (e) 160 s. E, S, and P indicate concentration profiles of enzyme (LAP), substrate (L-leucine-*p*-nitroanilide), and product (*p*-nitroaniline), respectively. For simulation parameters see Table 1.

initially positioned behind the enzyme zone. Thus, the capillary was filled with running buffer solution, a plug (approximately 5 nl) of LAP was hydrodynamically injected at the anodic inlet of the capillary, and the anodic buffer reservoir was filled with L-leucine-*p*-nitroanilide. However, it has been observed in EMMA experiments that when reagents are metered adjacently, during the brief time period prior to the application of potential diffusional interpenetration of the reagent zones results in an interfacial accumulation of product [2,8–10]. This phenomenon was simulated by allowing the capillary to sit in the absence of potential prior to the application of the electric field. As a result, Fig. 1a depicts the initial 0.4 cm of capillary at the anodic inlet immediately prior to the application of po-

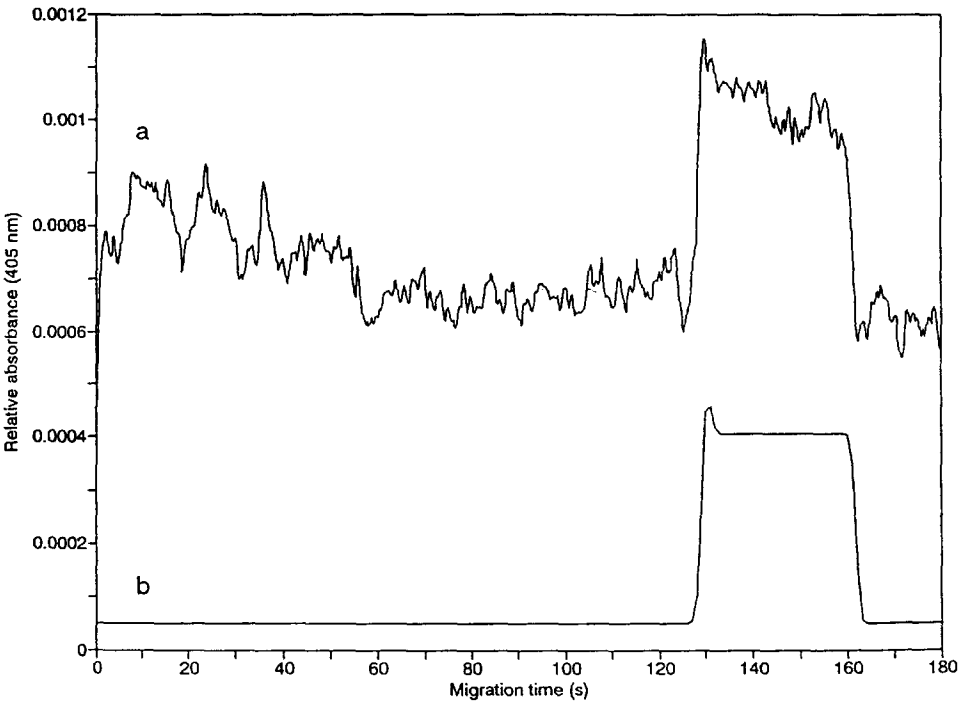

Fig. 2. (a) Experimental and (b) simulated zonal injection EMMA determinations of LAP. For experimental conditions and simulation parameters see text and Table 1.

tential. Substrate has diffused into the capillary from the anodic buffer reservoir and merged with the adjacent enzyme zone contained in the capillary thereby yielding an accumulation of reaction product.

Fig. 1b and c depicts the evolution of the plateau product profile characteristic of zonal injection EMMA determinations of enzymes performed at constant potential [2,8–10]. Under the influence of 300 V cm^{-1}, the substrate zone entering the capillary from the anodic buffer reservoir electrophoretically merged with the enzyme zone. Since the analyte was not depleted in the reaction, a relatively constant rate of product formation was observed. Furthermore, since the enzyme continually encountered fresh substrate due to the differential electrophoretic mobilities of LAP and L-leucine-*p*-nitroanilide, and the rate of reaction was relatively low, essentially no depletion of the substrate can be observed in Fig. 1b and c. However, because the product and enzyme also differed in electrophoretic mobility, *p*-nitroaniline was continually separated from the LAP zone and, thus, did not accumulate in the vicinity of the analyte under the influence of an electric field. As a result, the product profile was a plateau, and, since the enzyme zone displayed a lower net migration velocity than the product, *p*-nitroaniline led the LAP region through the capillary with the interfacial product appearing at the leading edge of the plateau. Fig. 1b and c illustrates that, as the potential was maintained, the width of the plateau product profile increased, the plateau height remained constant, and the interfacial accumulation of product became less discernible due to diffusion.

Fig. 1d and e illustrates the determination of the temporal detection limits of the product profile. As seen in Fig. 1d, the first product to reach the detection position (indicated by vertical dashed line at 19.4 cm) at approximately 130 s of applied potential was the interfacial product accumulation at the leading edge of the plateau. The final observed product depicted in Fig. 1e was that which formed as

the enzyme zone migrated past the detection position at approximately 160 s. Although the LAP and L-leucine-*p*-nitroanilide zones remained engaged, and, thus, the reaction continued throughout the enzyme's traversal of the capillary, product generated by LAP beyond the detection position could not be observed. Fig. 2 depicts an experimental determination of LAP as well as the simulated electropherogram obtained by monitoring the concentration profile of *p*-nitroaniline at the array element corresponding to the detection position. The experimental and simulated electropherograms offer good agreement with respect to product migration times and the plateau profile's shape and height as well as the comigration of the interfacial accumulation with the leading edge of the plateau.

4.2. Simulation of moving boundary EMMA determination of LAP

Although EMMA methods have generally utilized zonal injections of analyte, our laboratory has recently reported the use of electrokinetic moving boundary sample introduction [8]. In this technique, the capillary is initially filled with the slower migrating enzyme or substrate while the faster migrating complementary enzyme or substrate is maintained in the inlet buffer reservoir. Thus, upon the application of an electric field, the faster migrating reagent entering the capillary from the inlet reservoir electrophoretically interpenetrates the slower migrating species contained in the capillary. This technique results in greater reagent overlap than zonal injections and, consequently, typically yields better than an order of magnitude higher concentration sensitivity.

Fig. 3 and Fig. 4 depict the simulation of the moving boundary EMMA determination of LAP previously described [8] employing the same enzymatic reaction as the zonal injection EMMA determination of LAP. The capillary was initially filled with enzyme solution while substrate was maintained in the anodic buffer reservoir. As previously described for the zonal injection method, product formed at the interface between the adjacent LAP and L-leucine-*p*-nitroanilide zones due to their diffusional interpenetration prior to the application of potential. This phenomenon is shown in Fig. 3a, which depicts the initial 0.2 cm of capillary at the anodic inlet immediately prior to the application of an electric field.

Fig. 3b and c illustrates the evolution of the triangular product profile characteristic of moving boundary EMMA determinations of enzymes [8]. Upon the application of 300 V cm^{-1}, the substrate zone electrophoretically merged with the enzyme region. However, in contrast to zonal injection EMMA for which the volume of overlap remains relatively constant throughout the engagement of the reagent zones, the reagent overlap in moving boundary EMMA increased as potential was maintained. As a result, the product profile was triangular in contrast to the plateau profile observed for the zonal injection method, and the interfacial accumulation comigrated with the apex of the triangular product profile rather than at the leading edge of the zonal injection's plateau profile. As seen in Fig. 3b and c, the width and height of the triangular product profile increased proportionally as the electric field was maintained while the interfacial accumulation became less obvious due to its diffusional band broadening.

Fig. 3d and e depicts the determination of the temporal detection limits of the triangular product profile. The first product to reach the detector in Fig. 3d is that which formed just as the leading edge of the substrate zone (i.e., the leading edge of the reagent overlap region) migrated past the detection position after approximately 108 s of applied potential. The last product that could be observed in Fig. 3e is that which formed as the trailing edge of the enzyme zone (i.e., the trailing edge of the reagent overlap region) was transported past the detector at about 160 s. Fig. 4 shows that the experimental and simulated electropherograms agreed well with respect to product migration times as well as the triangular product profile shape and height and comigration of the interfacial accumulation with the apex.

4.3. Simulation of EMMA determination of ethanol

Although the determination of enzymes has been of greatest interest, the EMMA methodology has also been utilized to determine substrates via en-

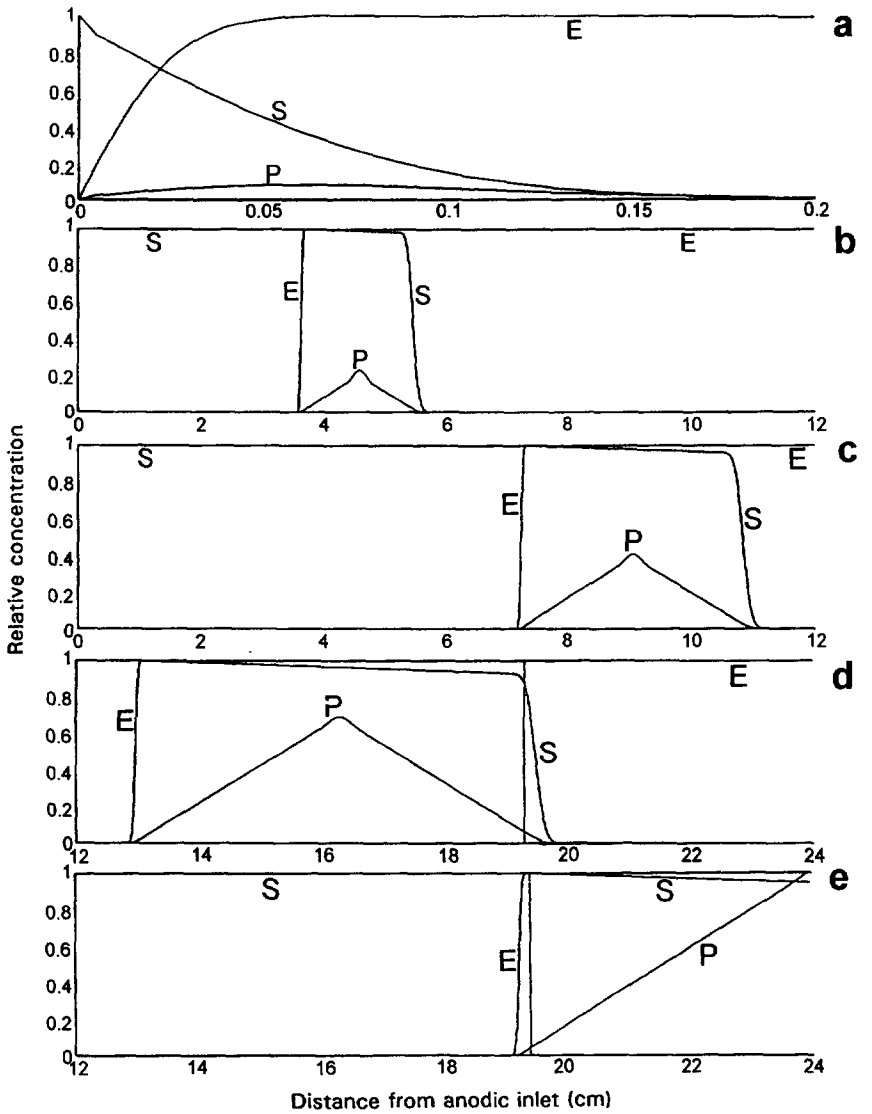

Fig. 3. Simulation of the moving boundary EMMA determination of LAP (a) immediately prior to the application of potential and following the application of 300 V cm^{-1} for (b) 30, (c) 60, (d) 108, and (e) 160 s. E, S, and P indicate concentration profiles of enzyme (LAP), substrate (L-leucine-*p*-nitroanilide), and product (*p*-nitroaniline), respectively. For simulation parameters see Table 1.

zymatic reactions. Fig. 5 and Fig. 6 depict the simulation of an EMMA determination of ethanol previously reported [10]. Ethanol was determined by its catalytic oxidation to acetaldehyde by alcohol dehydrogenase (ADH; EC 1.1.1.1) with the concurrent reduction of cofactor NAD^+ to NADH, which was monitored at its unique absorbance of 340 nm. This analysis illustrates the capability of the model to accommodate more complex kinetic systems by altering the form of Eq. 5. Rather than simple Michaelis–Menten kinetics, ADH displays an ordered bi–bi catalysis mechanism [26]

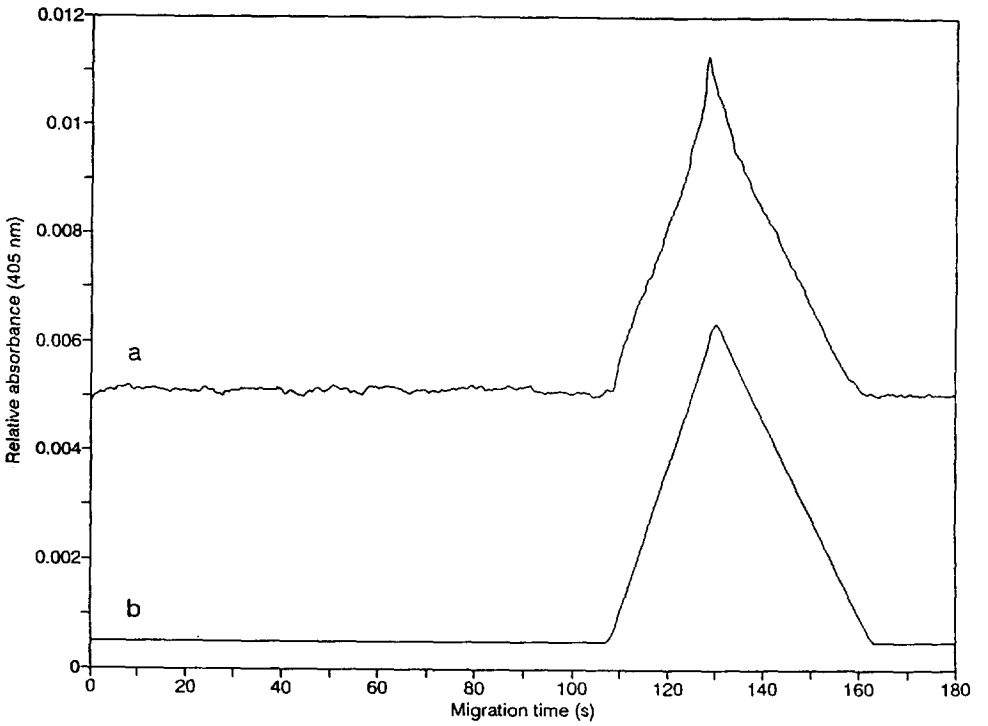

Fig. 4. (a) Experimental and (b) simulated moving boundary EMMA determinations of LAP. For experimental conditions and simulation parameters see text and Table 1.

$$\left[\frac{\delta[\mathrm{P}](x,t)}{\delta t}\right]_R = -\left[\frac{\delta[\mathrm{S}](x,t)}{\delta t}\right]_R = -\left[\frac{\delta[\mathrm{C}](x,t)}{\delta t}\right]_R = \frac{k_{\mathrm{cat}}[\mathrm{E}](x,t)}{1+\frac{K_{\mathrm{M,S}}}{[\mathrm{S}](x,t)}+\frac{K_{\mathrm{M,C}}}{[\mathrm{C}](x,t)}+\frac{K_{\mathrm{M,SC}}}{[\mathrm{S}](x,t)\,[\mathrm{C}](x,t)}} \quad (17)$$

where $[\mathrm{C}](x,t)$ is the concentration of cofactor at x and t, $K_{\mathrm{M,C}}$ is the Michaelis constant of the cofactor, and $K_{\mathrm{M,SC}}$ is the coupled Michaelis constant of the substrate and cofactor.

In this analysis, rather than inject the analyte zone adjacent to the analytical reagents, the capillary was initially filled with buffer solution containing ADH and NAD^+, and the anodic buffer reservoir was filled with buffer solution containing only NAD^+. An electric field of 100 V cm^{-1} was then applied for 60 s to create a gap lacking ADH. Approximately 3 nl of ethanol was then hydrodynamically injected, and the anodic buffer reservoir was returned to the NAD^+ solution. This reagentless gap was utilized to delay the engagement of the substrate and enzyme zones. In this manner, the time at which product is observed can be selectively controlled [10]. Since the substrate and enzyme were not introduced adjacently, no accumulation of product due to diffusional interpenetration of the reagents prior to the application of potential is seen in Fig. 5a, which depicts the capillary immediately prior to the application of potential. However, diffusional broadening of the analyte zone can be observed as well as diffusion of cofactor into the capillary from the anodic buffer reservoir. Under the influence of 250 V cm^{-1}, the greater net migration velocity of the ethanol zone allowed it to approach the ADH region. Thus, following 30 s of applied potential, the analyte zone

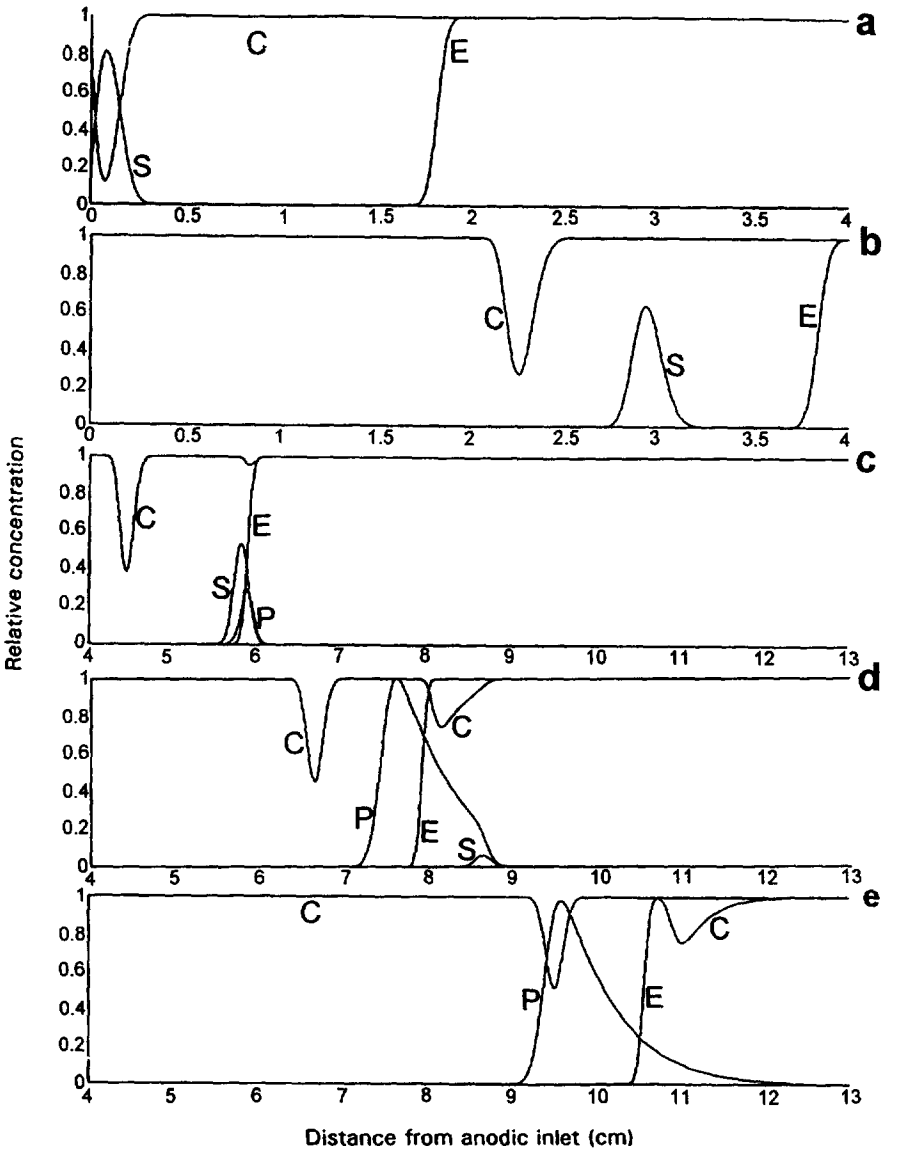

Fig. 5. Simulation of the zonal injection EMMA determination of ethanol (a) immediately prior to the application of potential and following the application of 250 V cm^{-1} for (b) 30, (c) 60, (d) 90, and (e) 130 s. S, E, C, and P indicate concentration profiles of substrate (ethanol), enzyme (ADH), cofactor (NAD^+), and product (NADH), respectively. For simulation parameters see Table 1.

had closed the initial 1.4 cm gap of Fig. 5a to approximately 0.6 cm in Fig. 5b. Furthermore, the ethanol zone had separated from the cofactor depletion zone resulting from the injection of substrate.

Fig. 5c–e depicts the evolution of the skewed product profile characteristic of EMMA substrate determinations [9–11]. In Fig. 5c, the substrate plug has engaged the enzyme zone following 60 s of applied potential at approximately 5.8 cm from the anodic inlet, and the initial product has formed. Ethanol and NADH differed in electrophoretic mobility, and, thus, NADH was continually transported from the vicinity of the ethanol as the reaction continued under the influence of an electric field. As

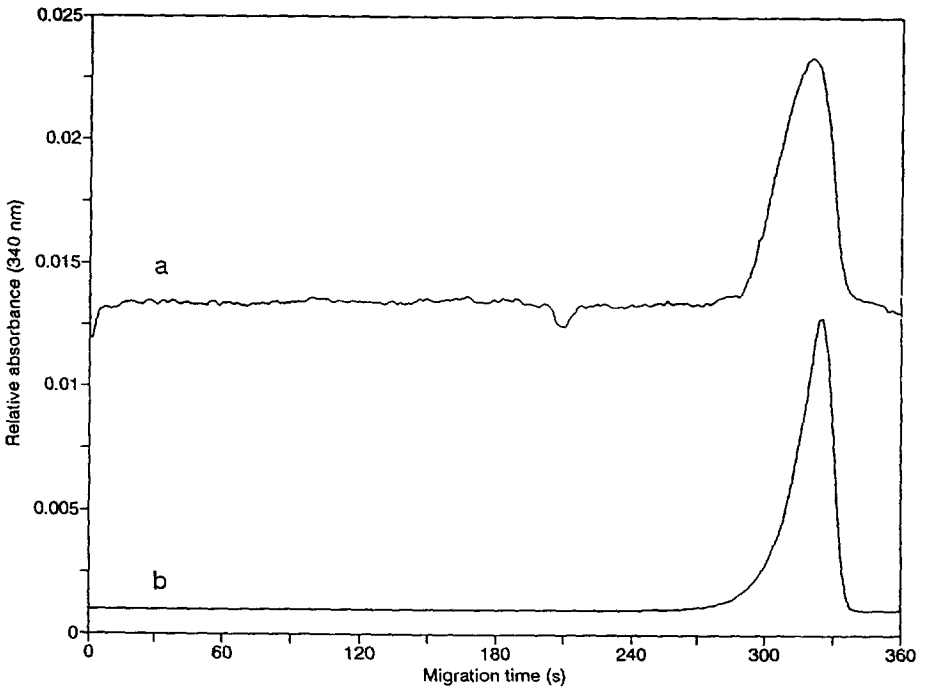

Fig. 6. (a) Experimental and (b) simulated zonal injection EMMA determinations of ethanol. For experimental conditions and simulation parameters see text and Table 1.

a result, the product profile was electrokinetically broadened as previously observed for the EMMA determination of LAP. However, unlike enzymatic analytes, ethanol was consumed in the reaction, and, consequently, the rate of product formation decreased as the engagement of the substrate and enzyme zones continued. This diminishing rate of NADH production yields the skewed product profile seen in Fig. 5d. Furthermore, in this analysis, significant reaction-induced depletion of the NAD^+ is observed (i.e., the depleted cofactor region at approximately 8.2 cm in Fig. 5d). By 130 s of applied potential, the ethanol zone is essentially consumed in Fig. 5e, and the complete skewed product profile is achieved. Thus, the remainder of the analysis time is required to transport the product profile to the detection position. In Fig. 6, the experimental and simulated electropherograms agree well with respect to product migration time and the general shape of the skewed product profile. The experimental product peak is broadened approximately 30% relative to that in the simulation. This is most probably due to the nonlinear electrophoretic behavior of the ternary complexes formed between the ethanol, acetaldehyde, NAD^+, and NADH with the alcohol dehydrogenase as governed by the bi–bi mechanism for which there is no account in the simulation. Errors in the kinetic constants used in the simulation may also contribute, but alone cannot account for the broadening as an exact simulation of the experimental electropherogram could not be made by adjusting the K_M and k_{cat} values in the simulation.

5. Conclusions

The computer implementation of the mathematical model has demonstrated good qualitative agreement with experimental EMMA electropherograms with respect to migration times and product profile shapes. Furthermore, the simulated concentration profiles provide insight into the evolution of the product profiles. Although the mathematical model

presented does not address potentially important effects of nonlinear behavior due to dissimilar local conductivities and band broadening due to the mechanism of complex formation, it does describe the principal roles played by electromigration, reaction kinetics, and diffusional band broadening. The program has proven valuable in our laboratory for such uses as evaluating the practicality of extracting kinetic parameters from the shapes of observed product concentration profiles; estimating the effects of solution viscosity upon diffusional band broadening of analyte and product zones and, therefore, the detection limits of EMMA analyses in which product is allowed to accumulate in the absence of potential [2–5,7,9,10]; and identifying the areas and degrees of reagent depletion during EMMA determinations.

Acknowledgments

Financial support was received from the National Institute of Health (Grant 5R02 GM51574-02) and PerSeptive Biosystems.

References

[1] F.E. Regnier, D.H. Patterson and B.J. Harmon, Trends Anal. Chem., 14 (1995) 177.
[2] J. Bao and F.E. Regnier, J. Chromatogr., 608 (1992) 217.
[3] D. Wu and F.E. Regnier, Anal. Chem., 65 (1993) 2029.
[4] K.J. Miller, I. Leesong, J. Bao, F.E. Regnier and F.E. Lytle, Anal. Chem., 65 (1993) 3267.
[5] D. Wu, F.E. Regnier and M.C. Linhares, J. Chromatogr. B, 657 (1994) 357.
[6] L.Z. Avila and G.M. Whitesides, J. Org. Chem., 58 (1993) 5508.
[7] Q. Xue and E.S. Yeung, Anal. Chem., 66 (1994) 1175.
[8] B.J. Harmon, I. Leesong and F.E. Regnier, J. Chromatogr. A, 726 (1995) 193.
[9] B.J. Harmon, D.H. Patterson and F.E. Regnier, Anal. Chem., 65 (1993) 2655.
[10] B.J. Harmon, I. Leesong and F.E. Regnier, Anal. Chem., 66 (1994) 3797.
[11] B.J. Harmon, D.H. Patterson and F.E. Regnier, J. Chromatogr. A, 657 (1993) 429.
[12] H.-T. Chang and E.S. Yeung, Anal. Chem., 65 (1993) 2947.
[13] D.H. Patterson, B.J. Harmon and F.E. Regnier, J. Chromatogr. A, 662 (1994) 389.
[14] S. Liu and P.K. Dasgupta, Anal. Chim. Acta, 268 (1992) 1.
[15] S. Liu and P.K. Dasgupta, Anal. Chim. Acta, 283 (1993) 739.
[16] P.K. Dasgupta and S. Liu, Anal. Chem., 66 (1994) 1792.
[17] E.V. Dose and G.A. Guiochon, Anal. Chem., 63 (1991) 1063.
[18] R. Aebersold and H.D. Morrison, J. Chromatogr., 516 (1990) 79.
[19] P. Gebauer, W. Thormann and P. Bocek, J. Chromatogr., 608 (1992) 47.
[20] C. Schwer and F. Lottspeich, J. Chromatogr., 623 (1992) 345.
[21] Y.-H. Chu, L.Z. Avila, H.A. Biebuyck and G.M. Whitesides, J. Med. Chem., 35 (1992) 2917.
[22] L.Z. Avila, Y.-H. Chu, E.C. Blossey and G.M. Whitesides, J. Med. Chem., 36 (1993) 126.
[23] Y. Walbroehl and J.J. Jorgenson, J. Microcolumn Sep., 1 (1989) 41.
[24] H. Hanson and M. Frohne, Methods Enzymol., 45 (1976) 504.
[25] C.J. Dickenson and F.M. Dickinson, Biochem. J., 147 (1975) 303.
[26] C.C. Wratten and W.W. Cleland, Biochemistry, 2 (1963) 935.